21st AIAA Aerodynamic Decelerator Systems Technology Conference and Seminar
23 - 26 May 2011, Dublin, Ireland

AIAA 2011-2573

Shipboard Landing Challenges for Autonomous Parafoils

Charles W. Hewgley* and Oleg A. Yakimenko†
Naval Postgraduate School, Monterey, CA, 93943-5107
Nathan J. Slegers‡
University of Alabama, Huntsville, AL 35889-0266

This paper examines some of the challenges that must be overcome if future aerial delivery systems are to have the capability to land on the flight deck of a ship underway. The unique aspects of trajectory planning for landing on a ship's flight deck are first examined, followed by formulation of the position estimation problem for a moving target. Some preliminary investigations into characterizing the wind over a moving landing platform at sea are then described. Finally, experimental results are presented for testing of a small prototype autonomous parafoil with a simple moving target on land.

Nomenclature

ADS	Aerial Delivery System
CAVR	Center for Autonomous Vehicle Research
CFD	Computational Fluid Dynamics
GPS	Global Positioning System
JPADS	Joint Precision Airdrop System
NPS	Naval Postgraduate School
UAH	University of Alabama in Huntsville
USV	Unmanned Surface Vehicle
WOD	wind-over-deck

I. Introduction

THE introduction of precision aerial delivery systems into the realm of military operations roughly a decade ago has enabled a rapidly-expanding set of logistic capabilities on the battlefield. Aerial Delivery Systems (ADSs) in use today such as the Joint Precision Airdrop System (JPADS) have enabled military ground forces to achieve widely distributed and nimble operations in challenging terrain such as the mountainous regions of Afghanistan.

Potential exists for the same sort of revolutionary changes that ground forces have enjoyed to be brought about in the maritime domain; however this potential is as yet unrealized. The unique additional challenges of landing an ADS on a ship underway at sea have delayed the adoption of advanced aerial delivery systems by naval forces. A significant capability that precision aerial delivery might provide in the maritime domain is that of vertical replenishment of naval vessels; previous work by the authors details the benefits of this innovation.[1]

The challenges of shipboard landing are not insurmountable. This paper details quantitative steps to solve the difficult landing problem. Section II examines characteristics of advanced guidance algorithms than can enable shipboard landing. Section III investigates various methods for the ADS to estimate the position of the target ship. Section IV addresses the challenge of winds and disturbed airflow over the superstructure of a ship underway. Section V summarizes recent experiments conducted by the Naval Postgraduate School (NPS) and the University of Alabama in Huntsville (UAH) starting to address the shipboard landing problem, and Section VI concludes with a look at future experimental plans.

II. Guidance Algorithms

The first challenge of shipboard landing for an autonomous parafoil that may come to mind is that the landing platform is moving; not simply according to the course and speed of the ship, but the landing platform's motion has

*Ph.D. Candidate, Department of Electrical and Computer Engineering, cwhewgle@nps.edu, Member AIAA
†Professor, Department of Systems Engineering, Code MAE/Yk, oayakime@nps.edu, Associate Fellow AIAA
‡Associate Professor, Department of Mechanical and Aerospace Engineering, slegers@mae.uah.edu, Senior Member AIAA

three axes of translation and three of rotation.[1] The motion of the landing platform will be addressed in Section III and is not the only challenge, and perhaps not even the most difficult challenge.

A naval ship presents a significant challenge to a landing aerial delivery system due to the superstructure immediately forward of the landing area that must be avoided. Figure 1 depicts side and plan views of the Republic of Korea Navy *Sejong the Great*-class destroyer showing the size of the helicopter landing area in relation to the large superstructure. This South Korean Navy ship is very representative of modern destroyer design. Figure 2 shows the plan view of the Republic of Korea Navy *Sejong the Great*-class destroyer alongside a U.S. Navy *Tarawa*-class amphibious assault ship to scale with a depiction of an aerial delivery system approach trajectory designed to land on the flight deck while avoiding the superstructure of the destroyer.

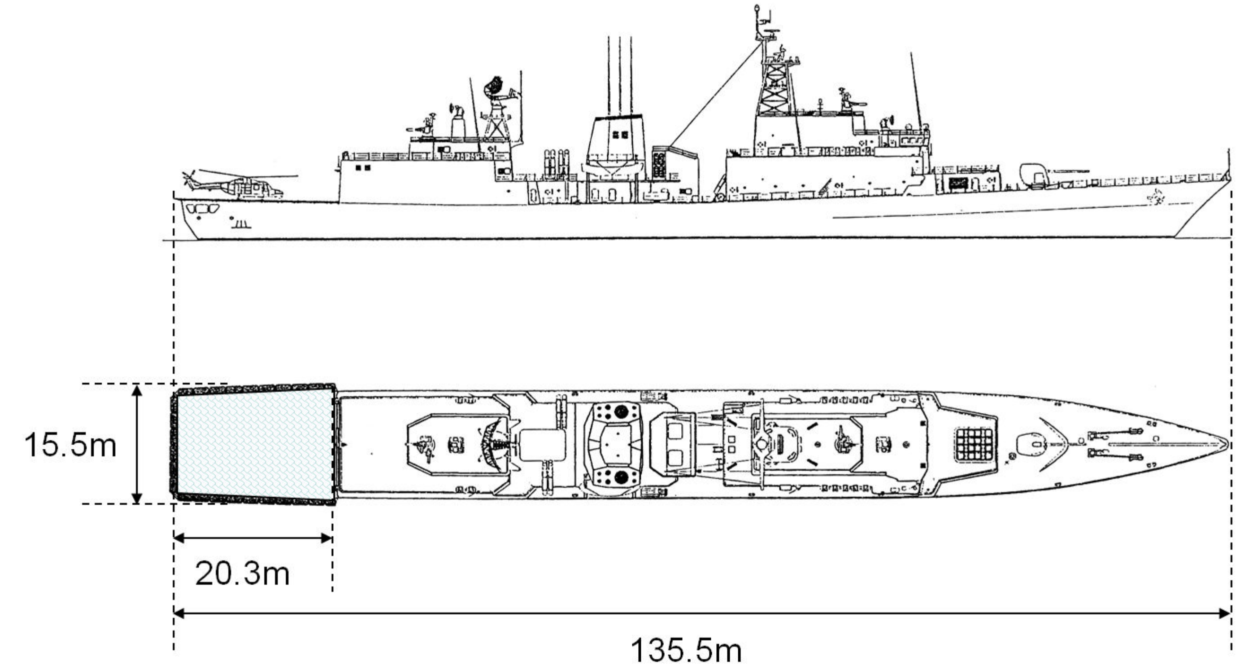

Figure 1. Republic of Korea Navy *Sejong the Great*-class destroyer demonstrates superstructure obstacles to ADS landing.

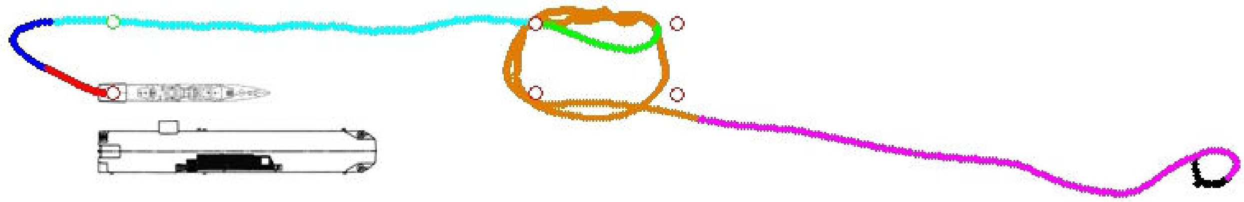

Figure 2. Example aerial delivery system flight path avoiding ship superstructure.

Shipboard landing of helicopters on smaller flight decks is a core competency of the U.S. Navy, and the standard operating procedure is to approach the flight deck from aft of the ship as depicted in Fig. 3.[2] For an ADS to be able to achieve shipboard landing, it must be able to replicate such a standard approach. Simple seeking of the coordinates of the landing platform or any sort of spiral approach from overhead will entail high risk of collision with the ship's superstructure.

The terminal guidance algorithm developed by Slegers and Yakimenko establishes a reference trajectory in the inertial reference frame.[3] In the case of the moving target (ship, submarine, *etc.*) this trajectory is tied to the moving target. Therefore, while planning the trajectory, it is possible to construct the trajectory so that the parafoil avoids, *e.g.,* a superstructure on the ship's deck. In Fig. 2, the superstructure of the ship is an island on the starboard side of the *Tarawa*-class ship. No other known guidance algorithm has the feature of trajectory planning for obstacle avoidance.

Another enhancement that may be necessary to land a parafoil accurately on a moving target is the capability to aim for a specific location or landing area on the target itself for the reason that different ships have different landing areas as a function of the ship's design. For example, U.S. Navy combatant ships are configured to have the flight deck located on the fantail aft, whereas some auxiliary ships may have the appropriate landing area on a forward deck, toward the bow of the ship. A few ships, notably the hospital ships USNS *Mercy* (T-AH-19) and USNS *Comfort*

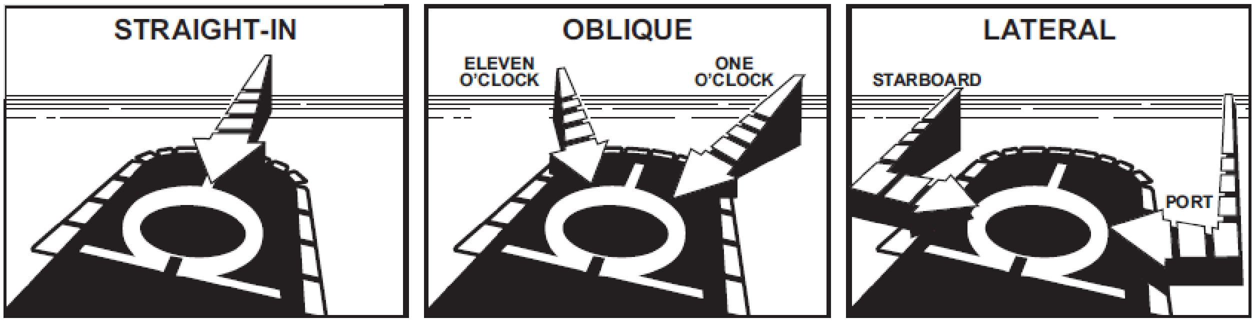

Figure 3. Types of standard shipboard approaches for helicopters.[2]

(T-AH-20), have helicopter flight decks positioned amidships. The position of the landing area longitudinally on the target ship as well as the height of the landing area above the waterline are two parameters that an advanced guidance algorithm will need in order to achieve shipboard landing.

Figure 4. USNS *Mercy* (T-AH-19) and USNS *Pecos* (T-AO 197) demonstrate various configurations for helicopter landing deck placement. Official U.S. Navy photograph by Chief Photographer's Mate E. G. Martens.

A third necessary characteristic of an advanced guidance algorithm for shipboard landing is that of having a guidance solution that can be recalculated very rapidly in response to changing conditions. The motion of the target ship is one condition that is always changing; heave and yaw motions of the landing platform in particular should be able to be handled by the guidance algorithm. The guidance algorithm detailed by Slegers and Yakimenko features an optimized final turn calculation that allows the algorithm to adjust the actual landing time of the parafoil as well as to recalculate the guidance solution on every iteration of the main software control loop, if necessary.[3]

III. Target Position Estimation

This section addresses two issues. The first is the issue of problem formulation, which is an adaptation of the original Snowflake terminal guidance formulation for a fixed target.[3] The second part of this section addresses the incorporation of information from a target position-reporting beacon for the possible application of landing an ADS on the deck of a cooperating ship for the purpose of resupply.

A. Problem Formulation

The original formulation of the terminal guidance problem by Slegers and Yakimenko in Ref. 3 described a three-dimensional, orthogonal frame with its origin centered at a fixed, non-moving target. The x-axis of this frame is pointed in the direction of an assumed prevailing wind direction, and oriented to point directly upwind. The z-axis is positive in the down direction, and the y-axis completes a right-handed, orthogonal triad.

In order to adapt this formulation for the moving target scenario, one must first define the starting time, labeled t_{start}. In this case, it will be assumed that the ADS follows a two-stage trajectory of which the first stage is a loitering stage in which the ADS flies a holding pattern upwind of the target while calculating the moment at which it should exit the loiter pattern and begin the approach for landing. Therefore, t_{start} will be defined as this moment of exiting the loiter pattern.

The target can then be described in two ways which are equated. The first way to define the target's location is by the change in its position along the x-axis from the moment the parafoil leaves the loitering phase to the moment the parafoil lands, *i.e.,* from t_{start} until landing. This value, labeled Δx_{T}, can be expressed as:

$$\Delta x_{\text{T}} = V_{\text{T}} \frac{z_{\text{start}}}{V_{\text{v}}^*} \tag{1}$$

where V_{T} is the velocity of the target and $z_{\text{start}}/V_{\text{v}}^*$ is the time duration from the moment the loitering phase is ended to the moment the parafoil lands. In this last expression, z_{start} is the altitude of the ADS at t_{start} and V_{v}^* is an assumed-constant vertical velocity. Another way to define the target's location is simply as the distance L from the ADS to the target along the x-axis. By equating the two expressions, it is stated that, commencing at t_{start}, the parafoil must move a distance L along the x-axis to land on a moving target that will be at position $x_{\text{T}} - V_{\text{T}} \frac{z_{\text{start}}}{V_{\text{v}}^*}$ assuming the target traveled at a constant velocity V_{T} in the negative x-direction from its starting location x_{T}. This equation can be expressed as:

$$L = x_{\text{T}} - \frac{V_{\text{T}}}{V_{\text{v}}^*} z_{\text{start}} \tag{2}$$

Equation (2) for L can be substituted into Eq. 39 of Ref. 3 and solved for z_{start} as:

$$z_{\text{start}} = V_{\text{v}}^* \frac{x_{\text{T}} + V_{\text{h}}^* (T_{\text{turn}} + 2T_{\text{app}}^{\text{des}})}{W - V_{\text{h}}^* + V_{\text{T}}} \tag{3}$$

which expresses the altitude at which the ADS must exit the loitering phase in order to achieve a landing on the moving target platform. In this expression, variable names are chosen to match those in Ref. 3: V_{h}^* is the steady-state no-wind horizontal velocity of the ADS, T_{turn} is the time required for the ADS to perform the 180° final approach turn, $T_{\text{app}}^{\text{des}}$ is the desired duration of the straight trajectory to the target immediately before landing, and W is an assumed constant wind speed from the surface up to the altitude of the ADS in the vicinity of the target.

B. Use of a Position-Reporting Beacon on the Target

One of the primary consequences of Eq. (3) is that both the position and velocity of the target, x_{T} and V_{T}, must be known or estimated. In the case of a cooperative target, such as the vertical replenishment scenario, it is reasonable to assume that the target ship could broadcast its position periodically using an automatic beacon. If the target is receiving reliable information for x_{T}, the problem then becomes one of estimating V_{T}. Taking simple differences between received values of x_{T} and dividing by the sampling interval in discrete time is likely to introduce much error into the estimation of V_{T}. In the sequel, a simple Kalman filtering algorithm is introduced in order to estimate V_{T}.

A first, very simple example problem can be devised in which the target platform is moving in a constant direction with nearly constant velocity and is equipped with a beacon that transmits the platform's position periodically with sampling interval T_s. The continuous-time system state equation for this simple system can be written as follows:

$$\dot{x}_1(t) = x_2(t) \tag{4}$$
$$\dot{x}_2(t) = 0 + w(t) \tag{5}$$

where state variables $x_1(t)$ and $x_2(t)$ represent the platform's position and velocity, respectively. Equations (4) and (5) can be written more compactly as:

$$\dot{\mathbf{x}}(t) = \mathbf{F}\mathbf{x}(t) + \mathbf{w}(t) \tag{6}$$

where

$$\mathbf{x}(t) = \begin{bmatrix} x_1(t) \\ x_2(t) \end{bmatrix} \qquad \mathbf{F} = \begin{bmatrix} 0 & 1 \\ 0 & 0 \end{bmatrix}$$

The process noise vector $\mathbf{w}(t)$ is a 2×1 column vector with only a non-zero entry in the second row, indicating that the process noise is applied only to the equation for the derivative of the velocity state variable. The process noise in this case represents a perturbation to acceleration and can be modeled as a normally distributed random variable with a mean of zero and a variance of σ_w^2.

The corresponding time-invariant, discrete-time system in which position is the measured output variable can be expressed in terms of state transition matrix Φ by the following difference equations:

$$\mathbf{x}[n+1] = \Phi\mathbf{x}[n] + \mathbf{w}[n] \tag{7}$$

$$\mathbf{z}[n] = \mathbf{H}\mathbf{x}[n] + v[n] \tag{8}$$

The measurement noise $v[n]$ is a feature of the discrete-time model only and can be used to represent inaccuracy in the position reporting beacon's transmissions. For example, the beacon inaccuracy can be modeled as a normally distributed random variable with zero mean and variance σ_v^2.

For the Kalman filter implementation, covariance matrices $\mathbf{Q}$ and $\mathbf{R}$ are required for process and measurement noise, respectively; for measurement noise, R is a scalar value equal to σ_v^2. For the discrete-time representation of process noise covariance matrix $\mathbf{Q}$, (assuming $\mathbf{Q}(t)$ is a constant matrix), a straightforward method such as is used in the book by Zarchan (Ref. 4) can be used to compute $\mathbf{Q}[n]$ as follows:

$$\mathbf{Q}[n] = \int_0^{T_s} \Phi(\tau)\mathbf{Q}\Phi^T(\tau)\, d\tau = \sigma_w^2 \begin{bmatrix} \frac{T_s^3}{3} & \frac{T_s^2}{2} \\ \frac{T_s^2}{2} & T_s \end{bmatrix} \tag{9}$$

where the state transition matrix Φ (assuming a time-invariant system) is computed by:

$$\Phi = e^{\mathbf{F}T_s} = \begin{bmatrix} 1 & T_s \\ 0 & 1 \end{bmatrix} \qquad \text{for } \mathbf{F} = \begin{bmatrix} 0 & 1 \\ 0 & 0 \end{bmatrix} \tag{10}$$

The matrix computed for $\mathbf{Q}[n]$ includes a multiplying factor which is the variance of the random variable element of $\mathbf{w}(t)$, σ_w^2.

Another covariance matrix that must be computed is the state estimate error covariance matrix $\mathbf{P}[n]$, which is defined as:

$$\mathbf{P}[n] = E\{\tilde{\mathbf{x}}^T\tilde{\mathbf{x}}\} \tag{11}$$

where the real-valued error signal $\tilde{\mathbf{x}}[n]$ is defined as:

$$\tilde{\mathbf{x}}[n] = \mathbf{x}[n] - \hat{\mathbf{x}}[n]. \tag{12}$$

The initial value of this matrix, denoted $\mathbf{P}[0]$, must be selected to reflect the confidence in the initial value of the state vector estimate, $\hat{\mathbf{x}}[0]$, although the performance of the Kalman filter will be relatively insensitive to the selected positive-definite matrix $\mathbf{P}[0]$.[4]

The implementation for the discrete-time Kalman filter can then be summarized in the following algorithm, noting that *a priori* values, which are those made before the latest measurement has been incorporated, are denoted by a superscript $-$ symbol, and the *a posteriori* values, those calculated after incorporating the latest measurement, are denoted by a superscript $+$ symbol.

1. Calculate the *a priori* error covariance matrix:

$$\mathbf{P}^-[n] = \Phi[n-1]\mathbf{P}^+[n-1]\Phi^T[n-1] + \mathbf{Q}[n-1] \tag{13}$$

2. Calculate the *a priori* state estimate:

$$\hat{\mathbf{x}}^-[n] = \Phi[n-1]\hat{\mathbf{x}}^+[n-1] \tag{14}$$

3. Calculate the Kalman gain:

$$\mathbf{K}[n] = \mathbf{P}^-[n]\mathbf{H}^T[n]\left[\mathbf{H}[n]\mathbf{P}^-[n]\mathbf{H}^T[n] + R[n]\right]^{-1} \tag{15}$$

4. Calculate the *a posteriori* state vector estimate using the latest measurement $\mathbf{z}[n]$:

$$\hat{\mathbf{x}}^+[n] = \hat{\mathbf{x}}^-[n] + \mathbf{K}[n]\left[\mathbf{z}[n] - \mathbf{H}[n]\hat{\mathbf{x}}^-[n]\right] \tag{16}$$

5. Calculate the *a posteriori* error covariance matrix:

$$\mathbf{P}^+[n] = [I - \mathbf{K}[n]\mathbf{H}[n]]\,\mathbf{P}^-[n] \tag{17}$$

IV. Winds Over the Landing Platform

As explained in other work by the authors,[5] the wind disturbance during the landing phase of flight for small ADSs is one of the major challenges for achieving an accurate landing on a fixed target on land. The challenge is magnified when examined in the context of an ADS attempting to land upon a moving platform at sea. Part of the challenge is with the relative wind over the landing deck, which is sometimes abbreviated as "WOD" for wind-over-deck. This term describes the air flow velocity that a sensor fixed to the landing platform would measure due to the combined effects of the prevailing wind and the motion of the platform.

In helicopter operations, the preferred relative wind for landing comes from within 30° of the ship's heading.[2] The relative headwind allows the landing helicopter to generate more lift at a lower approach speed of the helicopter relative to the ship than if the relative wind were from astern. The approach of an ADS to a landing platform aboard a ship is much different than that of a helicopter, primarily due to the much lower forward velocity of a parafoil compared to a helicopter on approach. In fact, it may be the case that a landing ADS would be better served by the target ship steering to minimize the relative wind, rather than steering to create a relative headwind as is traditional with helicopter operations. With the relative wind minimized, or even from astern the ship, the ADS would have a higher velocity relative to the ship, and the likelihood would be smaller that the ship would "outrun" the ADS as it attempted to land.

In order to characterize the relative wind environment for possible at-sea experiments involving the NPS/UAH Snowflake ADS, preliminary measurements of relative wind were gathered during underway operations of the SeaFox Unmanned Surface Vehicle (USV), operated by the NPS Center for Autonomous Vehicle Research (CAVR). An image of the SeaFox underway is shown in Fig. 5. Relative wind data were recorded using a small portable weather and wind speed meter attached to the boat's instrumentation mast. The boat's motion relative to an inertial frame of reference was determined using Global Positioning System (GPS) receiver information recorded at a rate of 0.5 Hz.

Figure 5. SeaFox USV underway on the Sacramento River.

Figure 6 shows an example of the velocity of the SeaFox USV measured by GPS along with the wind speed measured by the portable wind speed meter while operating in Monterey Bay, California. These three plots show three different portions of the test mission: the SeaFox standing at anchor (top plot), underway into the prevailing wind direction (middle plot) and underway with the wind astern (bottom plot). These plots show both the boat speed data as recorded by the on-board GPS receiver and winds as estimated by the Kestrel weather station. The wind data recorded while the boat stood at anchor is a measure of the prevailing wind velocity on the surface of the bay. The actual winds (over the water) for the second and third plot should be computed as a difference between the boat speed and what was measured by the Kestrel (in the moving system of coordinates). As seen in both cases the winds over the water were actually of the order of $1\,\mathrm{m/s}$ to $2\,\mathrm{m/s}$.

Another challenge inherent to landing on a moving platform at sea is turbulent airflow caused by the ship's superstructure. Characterization and visualization of the "airwake" of a ship underway as been the subject of some research, particularly for the application of helicopter operations; the article by Lee *et al.* contains a survey.[6] These studies often

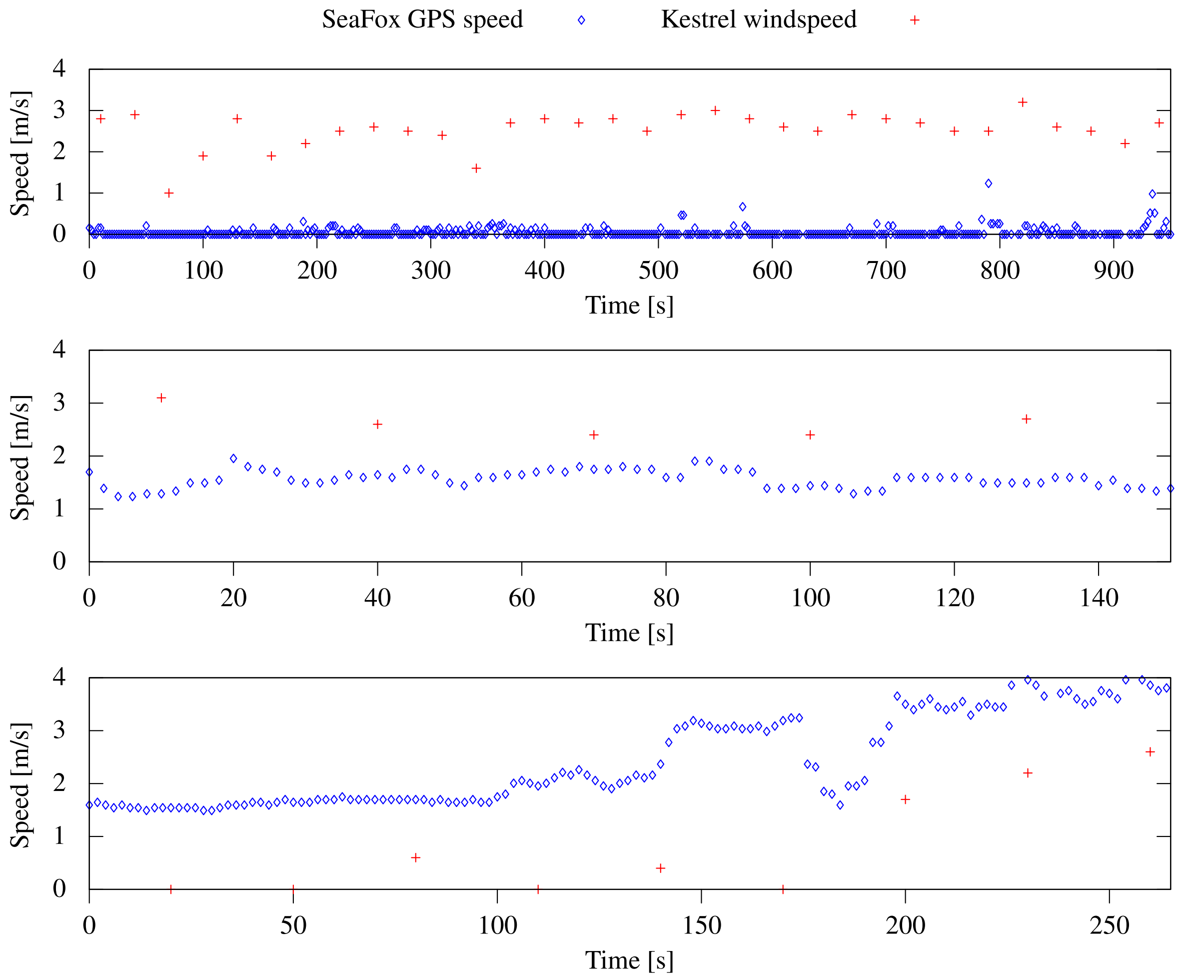

Figure 6. Example of boat velocity measurements and wind speed measurements.

rely on Computational Fluid Dynamics (CFD) in order to predict the flow field around the ship's superstructure; however, one recent research project at the U.S. Naval Academy is correlating CFD results with flow field data gathered *in situ* on a 33 m training vessel that has been modified to include a scale model flight deck aft of the superstructure.[7] Figure 7 shows one example of correlation between CFD and *in situ* data, where black vectors represent the *in situ* data, and white vectors and the background color scale represent the CFD flow field. One prominent feature of Fig. 7 is the region of recirculating flow immediately aft of the superstructure. This region of disturbed flow, sometimes called a "burble" by pilots, presents a challenge to the helicopter pilot upon landing. The effect of this pattern of flow on a landing ADS remains to be seen and is a topic for further experimentation.

V. Field Experimentation

Two sets of initial experiments involving the Snowflake ADS seeking a moving target were conducted at McMillan Airfield (identifier CA62) on 23 February, 2011, and 2 May, 2011. The target in each case was a vehicle equipped with a beacon that broadcast at a rate of 0.5 Hz the vehicle's current latitude and longitude as measured by GPS. The Snowflake ADS received these transmissions using a 900 MHz radio serial data link. The Snowflake autopilot used a moving average algorithm that included the five most recently received beacon transmissions to calculate the target vehicle's velocity.

For the experimental trials, the target vehicle was driven at a constant velocity of approximately 1.5 m/s (or between three and four miles per hour) along runway 28, while the Snowflake ADS continuously adjusted its target coordinates based on received beacon transmissions. Figure 9 shows the Snowflake ADS and target vehicle trajectories from the second experimental period of 2 May. The figure depicts the Snowflake's trajectory in a three-dimensional view along with the target vehicle's trajectory. The target vehicle was moving to the northwest, opposite the direction of the wind vector shown in Fig. 9. For this trial, the Snowflake landed approximately 5 m behind the target vehicle on the runway; an image of the Snowflake on its final approach is shown in Fig. 10.

The Kalman filter algorithm of Section III was used to process the recorded position data from the beacon. The

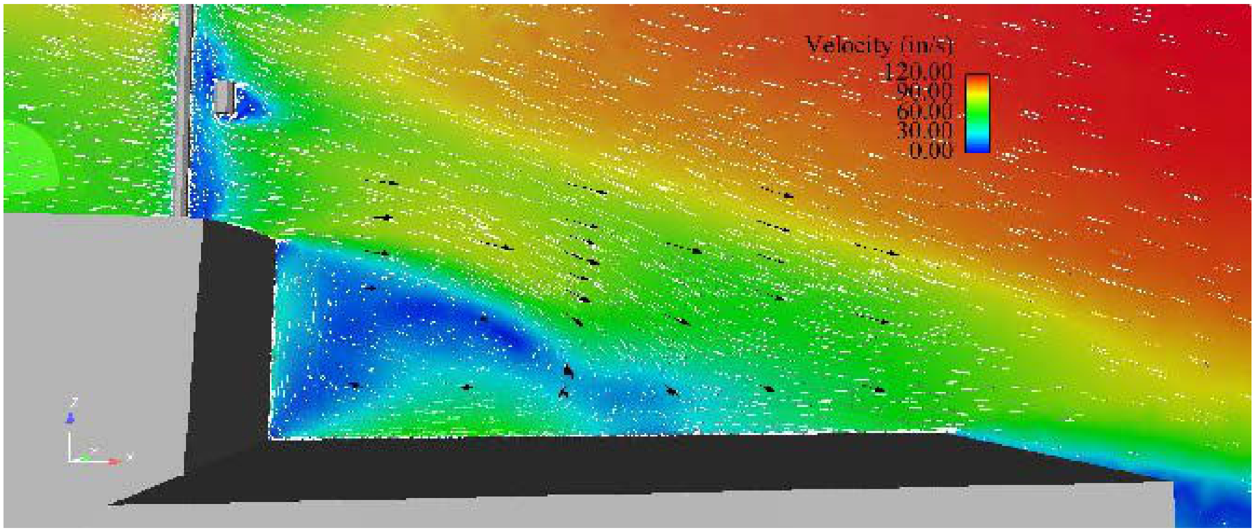

Figure 7. Normalized *in situ* data (black vectors) along with 7 knots time-averaged CFD data (white vectors and color scale) aft of the superstructure (courtesy of M. Snyder[7]).

Figure 8. Seamanship training craft of the "YP 676" class.

implementation of the filter algorithm had to account for the difference in sampling and transmission rates between the target beacon and the Snowflake autopilot. The main program loop of the Snowflake autopilot is executed at 4 Hz; but, the target position beacon made transmissions at 0.5 Hz. Because some of the target beacon's transmissions were missed (not transmitted and/or not received), the authors decided not to decrease the sampling rate at which the Snowflake autopilot checked for a beacon transmission. Instead, the Kalman filter algorithm was implemented such that for the instances in which a new beacon transmission was not received, the previous state estimate and state estimation error covariance matrix were extrapolated forward in time using Eq. (14). Figure 11 shows the results of the Kalman estimation for both experimental trials; 23 February and 2 May. This plot depicts the east-west (top plot) and north-south (bottom plot) components of the estimated target vehicle velocity. The true target vehicle speed was between 1.35 m/s (three miles per hour) and 1.79 m/s (four miles per hour). Because the East-West component of velocity is negative by convention (West), the slower target speed is represented by the upper horizontal line. Kalman filtering was performed separately on the latitude values of the beacon transmissions to produce a target velocity estimate in the North-South direction, and on the longitude values to produce an East-West target velocity estimate. Figure 11 shows that the velocity estimates for each component converged in approximately 20 s.

VI. Conclusion

The results of the moving target experiment have added encouraging evidence that shipboard landing of an ADS is an achievable possibility. The coupling of small aerial delivery systems with unmanned aerial vehicles will extend

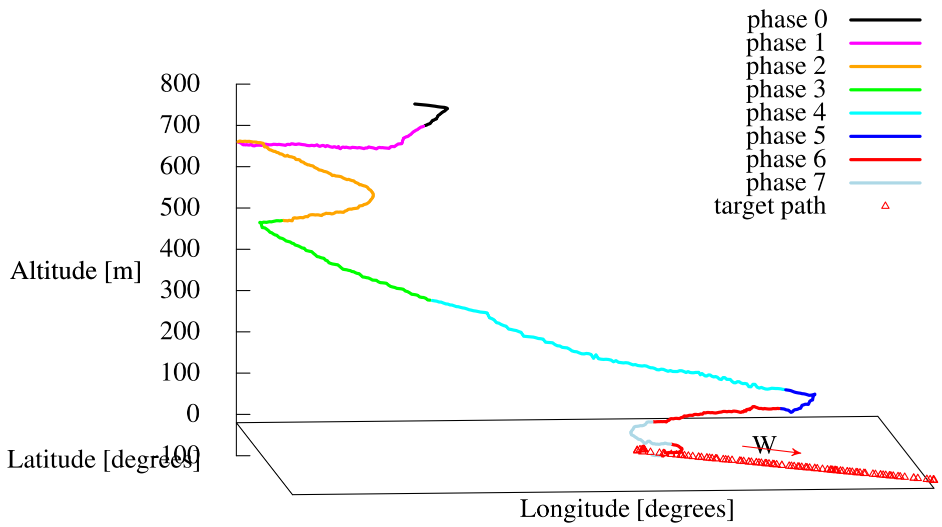

Figure 9. Snowflake ADS and moving vehicle target trajectories.

Figure 10. Snowflake ADS landing behind a moving target.

the possible uses of ADSs in the maritime domain even further.[8] Certainly, much work remains to be done for modeling realistic shipboard landing platforms and characterizing the wind environments around these vessels as they are underway. To this end, an initial set of maritime experiments is being planned for the summer of 2012 in conjunction with the U.S. Naval Academy. The scale flight deck on the instrumented YP vessel described in Section IV will provide an ideal maritime target for these experiments.

Acknowledgments

The authors wish to thank Sean Kragelund of the Naval Postgraduate School Center for Autonomous Vehicle Research and Eugene Bourakov of the Naval Postgraduate School Center for Network Innovation and Experimentation for their invaluable assistance in collecting the experimental data.

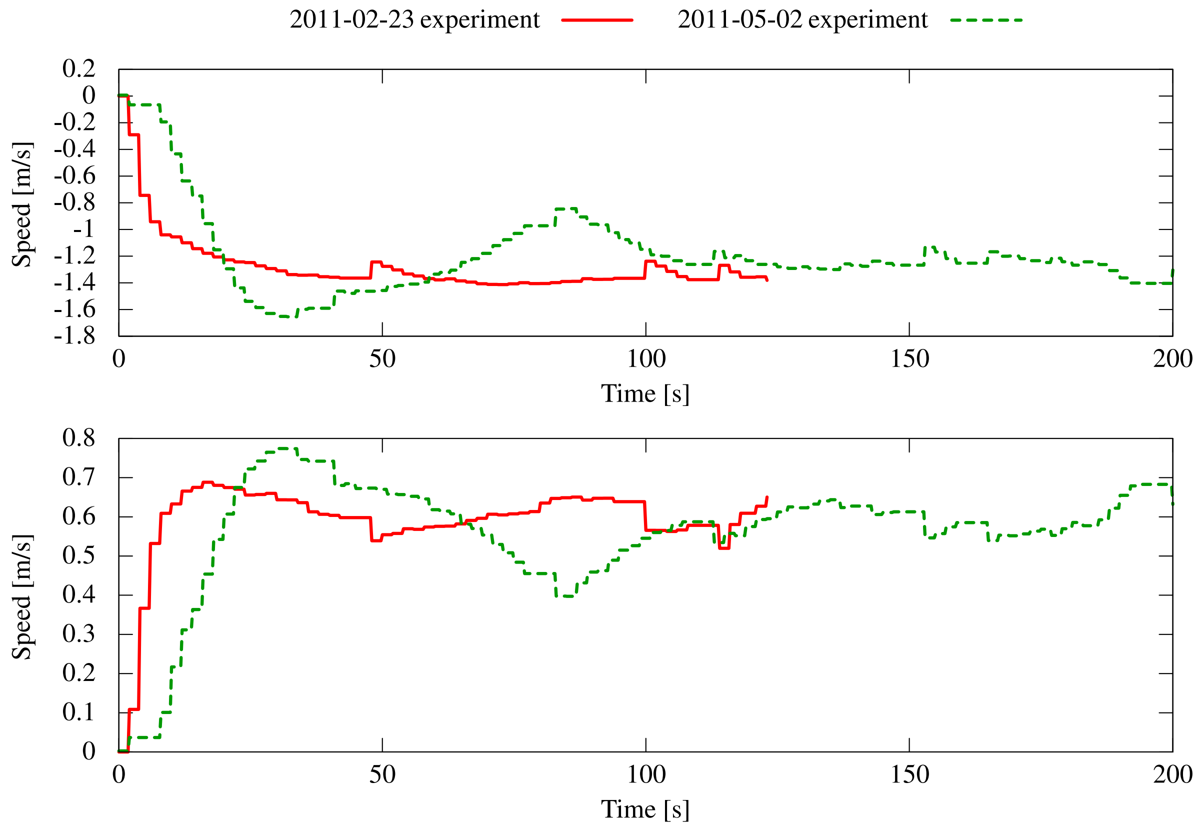

Figure 11. Kalman speed estimate of moving target in east-west direction (top plot) and north-south direction (bottom plot).

References

[1] Hewgley, C. W., and Yakimenko, O. A., "Precision Guided Airdrop for Vertical Replenishment of Naval Vessels," *Proceedings of the 20th Aerodynamic Decelerator Systems Technology Conference*, AIAA, Seattle, WA, 4–7 May 2009.

[2] U.S. Navy, "APP 2(F)/MPP 2(F) Volume I Helicopter Operations from Ships other than Aircraft Carriers (HOSTAC)," Allied Publication / Multinational Manual, Sept. 2001.

[3] Slegers, N. J., and Yakimenko, O. A., "Optimal Control for Terminal Guidance of Autonomous Parafoils," *Proceedings of the 20th Aerodynamic Decelerator Systems Technology Conference*, AIAA, Seattle, WA, 4–7 May 2009.

[4] Zarchan, P., and Musoff, H., *Fundamentals of Kalman Filtering: A Practical Approach*, Vol. 190 of *Progress in Aeronautics and Astronautics*, AIAA, Reston, VA, 2000.

[5] Hewgley, C. W., and Yakimenko, O. A., "Improved Surface Layer Wind Modeling for Autonomous Parafoils in a Maritime Environment," *Proceedings of the 21st Aerodynamic Decelerator Systems Technology Conference*, AIAA, Dublin, Ireland, 23–26 May 2011.

[6] Lee, D., Sezer-Uzol, N., Horn, J. F., and Long, L. N., "Simulation of Helicopter Shipboard Launch and Recovery with Time-Accurate Airwakes," *Journal of Aircraft*, Vol. 42, No. 2, March–April 2005, pp. 448–461. doi:10.2514/1.6786.

[7] Snyder, M. R., Shishkoff, J. P., Roberson, F. D., McDonald, M. C., Brownell, C. J., Luznik, L., Miklosovic, D. S., Burks, J. S., Kang, H. S., and Wilkinson, C. H., "Comparison of Experimental and Computational Ship Air Wakes for YP Class Patrol Craft," *Launch & Recovery Symposium*, American Society of Naval Engineers, Arlington, VA, 7–9 Dec. 2010.

[8] Yakimenko, O. A., Bourakov, E. A., Hewgley, C. W., Slegers, N. J., Jensen, R. P., Robinson, A. B., Malone, J. R., and Heidt, P. E., "Autonomous Aerial Payload Delivery System "Blizzard"," *Proceedings of the 21st Aerodynamic Delivery Systems Technology Conference*, AIAA, Dublin, Ireland, 23–26 May 2011.